THE JOURNAL OF PHYSICAL CHEMISTRY B

Article

pubs.acs.org/JPCB

Unravelling the Hydration Structure of ThX_4 (X = Br, Cl) Water Solutions by Molecular Dynamics Simulations and X-ray Absorption Spectroscopy

Riccardo Spezia,[†] Cesar Beuchat, [‡] Rodolphe Vuilleumier,[§] Paola D'Angelo,[∥] and Laura Gagliardi*[,⊥]

[†]CNRS, Laboratoire Analyse et Modélisation pour la Biologie et l'Environnement, UMR 8587 Université d'Evry Val d'Essonne, 91025 Evry Cedex, France

[‡]Department of Physical Chemistry, University of Geneva, 30 Quai Ernest Ansermet, CH-1211 Geneva, Switzerland

[§]Ecole Normale Supérieure, Département de Chimie, 24, rue Lhomond, 75005 Paris, France, and UPMC Univ Paris 06, 4, Place Jussieu, 75005 Paris, UMR 8640 CNRS-ENS-UPMC, France

[∥]Dipartimento di Chimica, Università di Roma "La Sapienza", P.le A. Moro 5, 00185 Roma, Italy

[⊥]Department of Chemistry and Supercomputing Institute, University of Minnesota, 207 Pleasant Street SE, Minneapolis, Minnesota 55455-0431, United States

Supporting Information

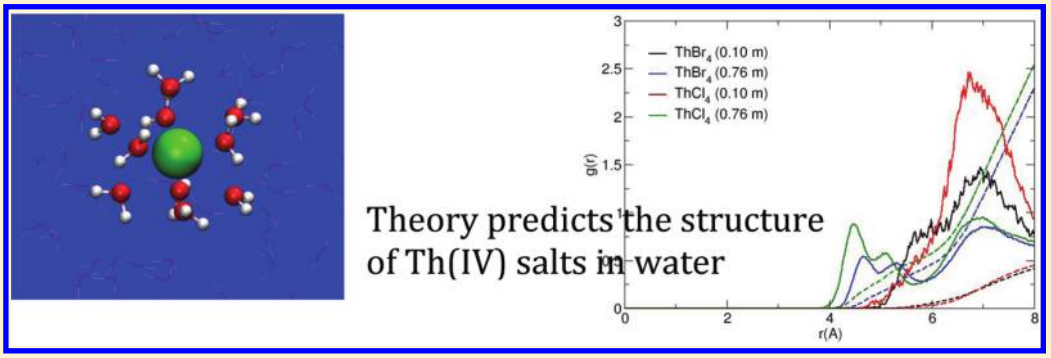

ABSTRACT: The hydration of Th(IV) in $ThCl_4$ and $ThBr_4$ water solutions at different salt concentrations was studied in order to understand the structure of Th(IV) in liquid water and the effect of Br^- and Cl^- anions on its hydration structure. Several theoretical methods were employed: density functional theory and classical molecular dynamics based on both semiempirical polarizable potentials and ab initio derived polarizable potentials. The results of the computations were combined with extended X-ray absorption fine structure (EXAFS) experimental data. The results of this study show that in pure water the Th−O distance of 2.45 Å corresponds to a first shell coordination number between 9 and 10. In the salt solutions, while Br^- does not affect directly the hydration of Th(IV) also at relatively high concentrations, Cl^-, on the other hand, is more structured around Th(IV), in agreement with recent high-energy X-ray scattering experiments. Counterions, even at relatively high concentrations (0.8 m), do not enter in the first solvation shell of Th(IV), but they induce an increase of water molecules in the first and second hydration shells of Th(IV).

1. INTRODUCTION

The understanding of hydration properties of ions is the first step in studying their reactivity in water. In particular, properties like ion−water distances and coordination numbers of solvation shells are at the center of both theoretical and experimental studies.[1−4] Recently, several classical molecular dynamics (MD) simulations have been successfully performed on very heavy metals, i.e., lanthanoids or actinoids, with newly developed intermolecular potentials able to correctly describe those ions in liquid water.[5−22] Density functional theory (DFT) has also been employed to describe hydrated lanthanoid and actinoid clusters of increasing dimensions,[23−28] in combination with continuum solvation methods[29−34] and explicit solvation with periodic boundary conditions to simulate bulk water—this last in conjunction with molecular dynamics.[18,35−41]

Thorium is of particular interest because it can be used as a combustible for nuclear power plants.[42] This could in principle lead to nuclear energy based on a more abundant combustible and with less radioactive wastes.[43] It is thus important to understand its behavior in solution.

Thorium(IV) hydration has been studied experimentally[44−47] and theoretically,[12,48,49] but many questions are still unanswered. In particular, while it is well established that the

Received: October 27, 2011
Revised: May 9, 2012
Published: May 9, 2012

   dx.doi.org/10.1021/jp210350b | J. Phys. Chem. B 2012, 116, 6465−6475

Th−water first shell distance is 2.45−2.46 Å,[44−46] the coordination number is not yet uniquely defined. EXAFS (extended X-ray absorption fine structure) and HEXS (high energy X-ray scattering) experiments have provided values in the 8−12 range,[44−47] and recent classical MD simulations[12] have reported two values, 8 and 8.5, that correspond to small changes of one force field parameter (and consequently of the Th−water distance). Previous simulations[48,49] in which the first hydration shell was kept fix to nine water molecules[48] predicted a Th−O distance of 2.54 Å.

Some recent experiments by Soderholm and co-workers[46] have shown that, for $ThBr_4$ in water, the Th(IV) hydration structure is independent of the salt concentration (up to about 0.7 m), suggesting that Br^- is not structured around Th(IV). On the other hand, for $ThCl_4$ in water, Cl^- interacts more strongly with the cation,[50−52] and large angle X-ray scattering measurements give strong indications for an inner sphere complex in liquid water.[47]

Given the interest in the topic and the uncertainty that still remains to be solved, we have undertaken a computational study aimed at a deeper understanding of the Th(IV) hydration structure and the differences between $ThCl_4$ and $ThBr_4$ salts at different concentrations. We employed a suite of theoretical methods, namely, DFT-based molecular dynamics (within the Car−Parrinello scheme[53]) and two polarizable-potential-based[6,54,55] classical molecular dynamics.

In recent years, radial distribution functions $g(r)$ obtained from MD simulations have been used as models for the interpretation of the EXAFS experimental data. The direct comparison between the EXAFS theoretical signal obtained from the MD $g(r)$'s and the experimental data can be used to test the accuracy of the theoretical models used in the simulations. The application of EXAFS is particularly interesting for simple systems, such as ions in solution. In this case, the small number of interaction functions required in the simulations allows each function to be checked and modified on the basis of the EXAFS experimental data, if necessary. This procedure has been followed for several cations, including Cm^{3+},[18] Cf^{3+},[56] and lanthanoids(III).[57] In a recent study, we have combined EXAFS and polarizable MD simulations to obtain effective ionic radii for the whole lanthanoid series in water.[58] In the present work, we have used this approach to investigate the Th(IV) hydration properties.

The paper is organized as follows. In section 2, we describe the details of the computations and of the data analysis. In section 3, we report the results of the study and the discussion, and in section 4, the conclusions.

2. METHODS

2.1. DFT-Based Simulations. DFT-based molecular dynamics within the Car−Parrinello scheme, CPMD, employs plane-waves (PWs) to describe the electronic wave function of the system. Only valence electrons are treated explicitly, while the core electrons are described by pseudopotentials (PPs). We used standard Troullier−Martins PPs.[59] The O and H valence/core partition is well studied, and the parameters have been previously obtained. For Th, we developed a semicore Troullier−Martins PP as follows. The reference configuration used to generate the PP for Th was Th(IV): $[Rn]5f^0 6d^0 7s^0$. The orbitals 6s, 6p, 6d, and 5f were included in the PP with cutoffs of 1.34, 1.59, 2.31, and 1.09 au, respectively. When using this PP with PWs, the semilocal Kleinman−Bylander form was used with the p channel as the local channel.[60]

Th(IV) was immersed in a box of 64 water molecules. Periodic boundary conditions (PBC) were employed in all cases to mimic the liquid phase. The cutoff value for the plane-waves was set to 110 Ry. The fictitious mass of the electronic wave function was chosen to be 150 au with a time step to numerically integrate the motion equation of 2 au (=0.048378 fs). The BLYP[61,62] functional was used. All the systems were previously equilibrated for 3 ns via classical molecular simulations at 300 K by using the classical potential described in the following (section 2.2).

In the CPMD simulations, a box with side equal to 12.43 Å was used. This corresponds to the size employed in a pure water calculation with 64 water molecules at ambient pressure and a density of 1 g/cm^3. By including the Th^{4+} cation, the density becomes 1.197 g/cm^3. This setup, which assumes that the partial molar volume of the cation is zero, is often used when simulating highly charged cations (see, for example, the simulation of Cm^{3+} in water by Atta-Fynn et al.[18]). A partial molar volume was employed by Yaziev and Helm when simulating Gd^{3+} and 56 water molecules,[41] which gave a total density of 1.224 g/cm^3. The partial volume of Th^{4+} as estimated by Hovey[63] from studying $Th(ClO_4)_4$ dilute solutions is negative, −60 cm^3/mol, probably due to strong electrostriction. Using such partial molar volume would lead to a total density for a system of 64 water molecules and one Th^{4+} of 1.266 g/cm^3. We thus decided not to use a partial molar volume for Th^{4+} because it would not make a significant difference (within statistical fluctuations) in terms of total density (1.197 g/cm^3 instead of 1.266 g/cm^3).

As reported in Table S1 of the Supporting Information, varying the box edge in reasonable ranges does not affect first hydration shell properties. One should also bear in mind that a simulation with only 64 H_2O molecules accurately describes only the first hydration shell, and not the second and third hydration shells. This is still useful because first shell properties can be compared directly with EXAFS data. Moreover, we should notice that, even for a system with only 64 water molecules, the statistical fluctuations[64] on the volume at 300 K and 1 bar are ca. 63 Å^3, corresponding to an edge fluctuation of 0.14 Å, given the water isothermal compressibility,[65] $5\cdot10^{-5}$ bar^{-1}. Thus, even assuming the partial molar volume of Th^{4+} in DFT simulations to be of the same magnitude as the experimental one, our simulation box falls close to these statistical fluctuations. To ensure that the water surrounding Th^{4+} is at the correct state point, we compared the oxygen−oxygen radial distribution function (RDF) in the Th^{4+}−water simulation with that of the pure water simulation with the same CPMD setup (see Figure S1, Supporting Information). The two RDFs are similar. This result confirms that these simulations correspond to very close thermodynamics states (i.e., ambient conditions for liquid bulk water). Box size effects on the Th−O RDF are reported in Figure S2, Supporting Information. While the peak intensities are slightly affected, the radial distances are not. Thus, our box size represents a good compromise between accuracy and computational cost.

The CPMD simulations were then performed, and after 1 ps of equilibration, we obtained equilibrated trajectories for about 11 ps. A Nosé−Hoover thermostat[66] was used in order to simulate the NVT ensemble, where the temperature was set to 300 K.

dx.doi.org/10.1021/jp210350b | J. Phys. Chem. B 2012, 116, 6465−6475

Table 1. The Fitted Parameters for the Various Potentials (See eq 4)[a]

	K^{ct}	K^{ere}	a^{ct}	a^{ere}		K^{ere}	a^{ere}
Th−O	518.60	307323	0.328	3.115	Th−H	825240	12.960
Th−Cl	106.29	137268	1.122	2.128	Cl−H	7809718	13.139
Th−Br	16.150	149885	1.171	2.035	Br−H	10459241	18.060
Cl−O		2908377		4.12	Br−O	3895073	4.17

[a] K is expressed in kJ/mol and a in Å^{-1}.

Within this approach, we simulated three Th(IV)$_{aq}$ systems, by using three different starting configurations: (i) in the initial configuration, Th(IV) is surrounded by 8 water molecules in the first shell (called here CPMD-8); (ii) in the initial configuration, Th(IV) is surrounded by 9 water molecules in the first hydration shell (CPMD-9); and (iii) in the initial configuration, Th(IV) is surrounded by 10 water molecules in the first hydration shell (CPMD-10). All the DFT-based simulations were performed with the CPMD code.[67]

2.2. Semiempirical Force Field Development and Simulations. A semiempirical polarizable potential was developed for Th(IV) in pure water, by using the same approach as the one developed by one of us for lanthanoids(III) in water.[6] Following this model, the total interaction potential is modeled as a sum of different terms

$$V_{tot} = V_{elec} + V^{LJ}_{O-O} + V_{Th-O} \quad (1)$$

where V_{elec} is the electrostatic energy term composed by a Coulomb and a polarization term following Thole's induced dipole model.[68] For water, we used the TIP3P[69] water model modified into TIP3P/P[70] in order to include atomic polarization, as recently done in the studies of the lanthanoid(III)[6] and actinoid(III)[20] hydration. For Th(IV), we used the atomic polarizability calculated at the *ab initio* level, as described in section 2.3. V^{LJ}_{O-O} is the 12-6 Lennard-Jones potential describing the O−O interaction in the TIP3P model. V_{Th-O} accounts for the *non-electrostatic* Th−O interaction potential, for which we employed the Buckingham pair potential of the form

$$V_{Th-O} = A\exp(-Br) - \frac{C}{r^6} \quad (2)$$

where for A we used the same values used for lanthanoids(III) while B and C were modified to have the correct distance, using the same approach used in refs 20 and 58, namely, B = 3.396 Å^{-1} and $C = 4.364 \times 10^4$ kJ mol^{-1} Å^6.

The MD simulations of Th(IV) in water were carried out in the microcanonical NVE ensemble with the MDVRY code.[71] The extended Lagrangian method was employed to obtain induced dipoles during the dynamics.[72] The simulations were performed for one Th(IV) ion and 216 rigid water molecules in a cubic box at room temperature. A side of 18.64 Å was used. For the system with 216 water molecules and 1 Th^{4+} ion, this corresponds to a total density of 1.057 g/cm^3. By increasing the box size, the uncertainty due to the ion partial molar volume is reduced and larger boxes are thus preferable. Long-range interactions were calculated by using the smooth particle mesh Ewald (SPME) method.[73] A velocity-Verlet-based multiple time scale (MTS) was used with a time step of 1 fs. The system was first equilibrated at 298 K for 2 ps, and then, a production run was collected for 3 ns. All other simulation details are the same as reported previously.[6,20,74,75] In the following, we refer to these classical (polarizable) molecular dynamics simulations as CLMD-EL, where EL stands for extended Lagrangian.

2.3. NEMO Force Field Development and Simulations. We used the NEMO approach[55] to develop interaction potentials from quantum chemical calculations. With the NEMO approach, the hydration of Cm(III),[17] UO_2^{2+},[19] and $LnCl_3$ salts at different concentrations[14] was recently studied. All QM calculations were performed using MP2 with ANO-RCC basis sets of triple-ζ quality as implemented in Molcas 7.2.[76]

In the NEMO force field, the total interaction energy is written as the sum of five terms:[55]

$$E^{tot} = E^{ele} + E^{ind} + E^{disp} + E^{ere} + E^{ct} \quad (3)$$

The starting point for the construction of a NEMO potential is one quantum chemical calculation on each of the interacting subsystems, Th(IV), water, Cl^-, and Br^- in our case. From the wave function of the subsystems, a distributed set of charges, dipoles, and quadrupoles is calculated for each atom (although the quadrupoles are replaced by dipoles on atoms close to the side for the quadrupole in the actual simulations) by means of the LoProp method.[77] Local polarizabilities are also calculated with LoProp. Local multipoles and polarizabilities are used to estimate the electrostatic, E^{ele}, and induction interaction, E^{ind}, between the two subsystems. The dispersion interaction, E^{disp}, is calculated using a London-type formula.[55] These three terms are obtained directly from wave function properties of each subsystem. To determine the last two terms of eq 3 (the exchange repulsion energy, E^{ere}, and charge transfer energy, E^{ct}), the contributions from the first three terms in eq 3 are subtracted from the total interaction energy between the two subsystems obtained from *ab initio* calculations.

The sum of these two terms, $E^{ere} + E^{ct}$, is then fitted as a sum of interatomic exponential terms, which is used for the final construction of the NEMO potential

$$E^{ere} + E^{ct} = \sum_{i,j} (K^{ere}_{ij} e^{-a^{ere}_{ij} r_{ij}}) - K^{ct}_{ThO} e^{-a^{ct}_{ThO} r_{ThO}} - K^{ct}_{ThX} e^{-a^{ct}_{ThX} r_{ThX}} \quad (4)$$

The first term describes E^{ere}, and r_{ij} represents the distance between atoms i and j, where the sum runs over all interacting atom pairs. The following attractive terms describe the charge transfer, occurring only between the Th(IV) ion and the water oxygen and between the Th(IV) ion and the halogen anions (Br^- and Cl^-). The fitting parameters for the various species are reported in Table 1. For the water−water potential, the same repulsion parameters were used as those reported in ref 19.

As already discussed by Réal et al.,[12] while generating the interaction curve between an isolated Th(IV) ion and a water molecule, at a Th(IV)−H_2O distance longer than 3 Å, an electron transfer occurs and one has instead Th(III) and H_2O^+. In the NEMO potential, the sum of the two terms, $E^{ere} + E^{ct}$, which is fitted, represents a short-range interaction. The fitting was thus performed against the MP2 interaction energy curve

dx.doi.org/10.1021/jp210350b | J. Phys. Chem. B 2012, 116, 6465−6475

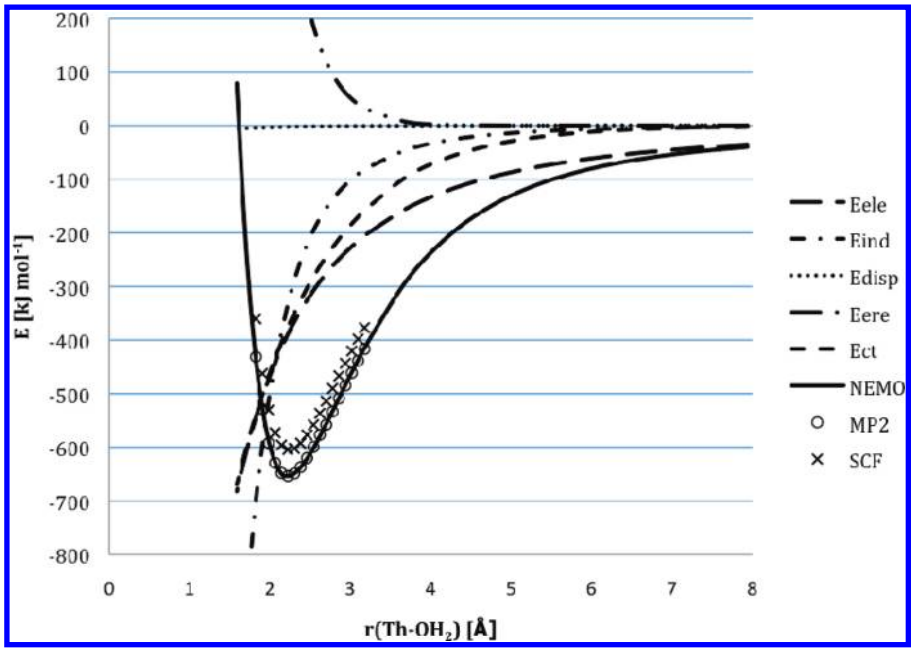

Figure 1. Th−water fitting curve. The interaction energy between one water molecule and Th(IV). The crosses and circles correspond to the quantum chemical calculations at the SCF and MP2 levels, respectively; the solid line is the full NEMO interaction potential fitting MP2 energies. Other lines correspond (as specified in the figure) to different contributions to the NEMO interaction potential, eqs 3 and 4 (see text for details).

only in the bonding region (between 1.8 and 3.2 Å), as shown in Figure 1. Longer-range interactions between Th^{4+} and H_2O are described by the other terms in eq 3. In the MP2 calculations, from which the NEMO-FF was built, a rigid water molecule was employed, so no hydrolysis could be observed. Note that, to generate the Th−water potential energy curve for the NEMO-FF, the geometry of the water molecule was taken from a prior DFT cluster calculation where no hydrolysis was observed.

For the generation of the potential between Th(IV) and Cl^- or Br^-, the MP2 interaction energy curves were computed from a starting configuration composed by four Cl^-/Br^- and one Th(IV) ion in a tetragonal geometry. Then, one Cl^-/Br^- was pulled apart from the Th^{4+} cation. The other three Cl^-/Br^- were kept at a fixed position and were taken into account during the fitting procedure.

The NEMO potential was then employed to perform molecular dynamics simulations by using the Molsim package.[78] For each system ($ThBr_4$ and $ThCl_4$), we considered two concentrations, a lower (0.1 m) one and a higher (0.8 m) one, similar to what was employed by Soderholm and co-workers.[46] The low concentration systems were composed by 1 Th^{4+}, 4 Br^- or Cl^-, and 497 water molecules, while the high concentration ones by 7 Th^{4+}, 28 Br^- or Cl^-, and 467 water molecules. Each system was first equilibrated via NpT simulations for about 1 ns by means of Berendsen's thermostat and barostat[79] by employing a target temperature and pressure of 300 K and 1 atm, respectively. PBC were applied to mimic the liquid phase, with Ewald summation, for which the parameters were set according to Kolafa's prescription[80] with a radial cutoff equal to 11 Å and a tolerance of 0.01 kJ/mol. After equilibration, trajectories were propagated for 3 ns.

In the following, these classical molecular dynamics simulations will be called CLMD-NEMO.

2.4. Experimental and Data Analysis. The EXAFS spectra were collected by Persson and co-workers and were previously reported in ref 45. However, for completeness, we report in the following the details of the sample preparation and EXAFS spectra that we used for analysis and comparison with simulations among the different samples prepared and analyzed in the original work.

Sample Preparation. Thorium(IV) nitrate pentahydrate, $Th(NO_3)_4{\cdot}5H_2O$ (Merck 99%), perchloric acid (Merck), and concentrated aqueous ammonia (25% by weight, Merck) were used as purchased. Octaaqua(κ^2O-perchlorato)thorium-(IV) perchlorate monohydrate, $[Th(H_2O)_8(ClO_4)](ClO_4)_3{\cdot}3H_2O$, was prepared by dissolving weighed amounts of $Th(NO_3)_4{\cdot}5H_2O$ in 5 M perchloric acid followed by precipitation of thorium hydroxide with addition of concentrated ammonia.[45,81,82] The obtained residue, hydrated thorium(IV) hydroxide, was washed with distilled water and dissolved in 11.6 M perchloric acid. The solution was then filtered through a paper filter and evaporated until a highly viscous concentrated solution, 2.94 M, ρ = 2.35 g cm^{-3}, was obtained.[45,81] A 1.06 M aqueous thorium perchlorate solution was prepared from the concentrated solution by dilution with 1.0 M perchloric acid. A pH value of −0.70 was reached. It is necessary to keep the pH below 1 at these concentrations to avoid hydrolysis. At this pH value and cation concentration, the Th(IV) ion is fully hydrated and no polynuclear hydrolysis species are present in solution.[45,81] Moreover, as shown by Johansson et al.[47] in perchlorate solutions, no inner-sphere complexes are formed and the geometry of the first coordination sphere does not depend on the salt concentration.

EXAFS Data Analysis. The EXAFS spectra were collected by Persson and co-workers and were previously reported in ref 45. We thus do not report the details of the EXAFS spectra for which the reader should go directly to ref 45. What is new in this work is the analysis of those data. EXAFS measurements of the aqueous solution of thorium(IV) perchlorate were performed at the Th L_3 X-ray absorption edge. The data were collected at the bending magnet beamline 2-3 at the Stanford Synchrotron Radiation Lightsource (SSRL), Stanford, CA, which operated at 3.0 GeV and a maximum current of 100

mA. The EXAFS station was equipped with a Si[220] double crystal monochromator. Higher order harmonics were reduced by detuning the second monochromator crystal to reflect 60% of maximum intensity at the end of the scans. Internal energy calibration was made with a foil of metallic thorium assigned to 16 300 eV. The measurements were performed in transmission mode, and three scans were averaged after energy calibration by means of the EXAFSPAK program package.[83]

For the hydration shell of cations, particularly those coordinating water at relatively long distances, the main contribution to the EXAFS signal is associated with the single scattering events that reflect a two-body interaction. Rather than using the usual discrete form of the EXAFS equation,[84] the signal is modeled as a function of the radial distribution function, $g(r)$, as[85]

$$\chi(k) = \int_0^\infty 4\pi\rho r^3 g(r) A(k, r) \sin[2kr + \phi(k, r)]\, dr \quad (5)$$

where $A(k, r)$ and $\phi(k, r)$ are the amplitude and phase functions, respectively, and ρ is the density of the scattering atoms. $\chi(k)$ theoretical signals can be calculated by introducing in eq 5 the model radial distribution functions obtained from the simulations. A comparison of the theoretical and experimental total $\chi(k)$ signals allows the reliability of the $g(r)$'s obtained from the simulation and consequently of the theoretical scheme and potentials used in the simulations.

The EXAFS theoretical signals were calculated by means of the GNXAS program, described in detail in refs 86 and 87. Phase shifts, $A(k, r)$ and $\varphi(k, r)$, have been calculated starting from one of the CPMD configurations, by using muffin-tin potentials and advanced models for the exchange-correlation self-energy (Hedin-Lundqvist). The values of the muffin-tin radii are 0.2, 0.9, and 1.8 Å for hydrogen, oxygen, and thorium, respectively. These radii correspond to an overlap between the thorium and oxygen atoms of about 10%. We checked that there are no detectable variations of the theoretical signals in the EXAFS region when the muffin-tin radii are reduced until tangency is reached. Inelastic losses of the photoelectron in the final state were accounted for by a complex potential. The imaginary part also includes a constant factor accounting for the core-hole width (7.13 eV).

Both Th−O and Th−H $g(r)$'s obtained from the simulations were used to calculate the single scattering first shell $\chi(k)$ theoretical signal, as the ion−hydrogen interactions were found to provide a detectable contribution to the EXAFS spectra of lanthanoid ions in aqueous solutions.[88] Conversely, recent investigations on Th(IV) aqueous solution have shown that multiple scattering effects within the first hydration shell of Th(IV) can be neglected.[45,81] The reduction amplitude, S_0^2, a factor accounting for a uniform reduction of the signal associated with many-body effects, was set equal to 1. The total $\chi(k)$ contribution which is the sum of the two-body signals from oxygen and hydrogen atoms was shifted in energy space to fit the experiment (E_0). The agreement between the theory and the experiment is then evaluated by the index of agreement between experimental ($\alpha_{exp}(E_i)$) and the theoretical ($\alpha_{theo}(E_i)$) points defined as

$$R = \sum_{i=1}^{N} \frac{[\alpha_{exp}(E_i) - \alpha_{theo}(E_i)]^2}{\sigma_i^2} \quad (6)$$

where N is the number of experimental points E_i and σ_i^2 is the variance associated with each experimental point $\alpha_{exp}(E_i)$. In most cases, σ_i^2 can be directly estimated from the experimental spectrum and a k^m weighting (with m = 2, 3, etc.) results in a good approximation.[87]

3. RESULTS

3.1. Diluted Solutions. We first discuss the results obtained for Th(IV) in pure water from CPMD and CLMD-EL simulations (two snapshots are shown in Figure 2 as an example) or diluted solutions (low concentration, 0.1 m) from CLMD-NEMO simulations and compare the simulation results with the EXAFS experimental data. In a previous investigation, the same EXAFS spectrum was analyzed by Persson et al.[45] using the standard data analysis procedure. The mean Th−O bond distance obtained from this analysis was of 2.451(3) Å, corresponding to a nine-coordinated Th(IV) ion, probably in ttp (tricapped trigonal prism) fashion even though monocapped square antiprismatic or other nine-coordinated configurations could not be excluded. The same Th−O bond distance was reported also in previous studies, but it was associated with higher coordination numbers.[44,46,89] It is important to emphasize that, if independent coordination models are not available, the uncertainty in the coordination numbers obtained from the standard EXAFS data analysis is too large for a conclusive determination of the geometry of hydration complexes. As a consequence, for structural studies on aqua ions in solution, the mean metal−oxygen bond length obtained from EXAFS analysis is a more reliable indicator of the coordination number than the direct determination of the number of coordinated ligands. A strategy often adopted to extract more accurate structural parameters from the EXAFS data is to use a combined MD-EXAFS approach. When MD simulations are not too much in disagreement with experimental evidence, the fitting process of the EXAFS data starting from the MD $g(r)$'s is similar to a minimization with constrained parameters and these conditions reduce meaningfully the uncertainty of the structural parameters. In the present investigation, the EXAFS experimental data have been analyzed using this approach.

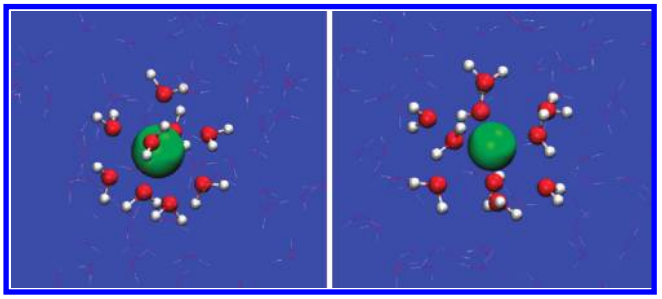

Figure 2. Snapshots of water solution simulations where Th(IV) is in green and water molecules in the first hydration shell are represented in ball and sticks, while the remaining bulk molecules are represented as lines. (left) CN = 9; (right) CN = 10.

The values for Th−O and Th−H $g(r)$'s obtained from CPMD and CLMD simulations, respectively, are shown in Figures 3 and 4, respectively. There is a well-defined first hydration shell and a second shell, not as well-defined as the first one. From CLMD $g(r)$'s, it is also possible to identify a third shell. The effect of Th(IV) up to a third shell is probably due to the high charge of the central ion (4+) that provides a long-range electrostatic attraction up to 7 Å. Note that a small peak in the third shell is also detected in the experimental pair

dx.doi.org/10.1021/jp210350b | J. Phys. Chem. B 2012, 116, 6465−6475

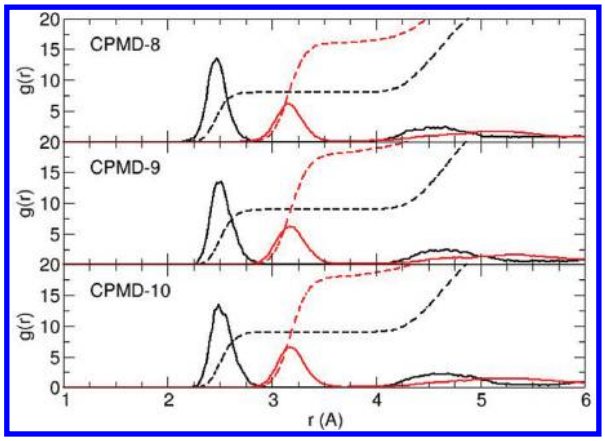

Figure 3. Th−water radial distribution function obtained from CPMD simulations. Th−O in black and Th−H in red. The integrated coordination numbers are also shown (dashed lines).

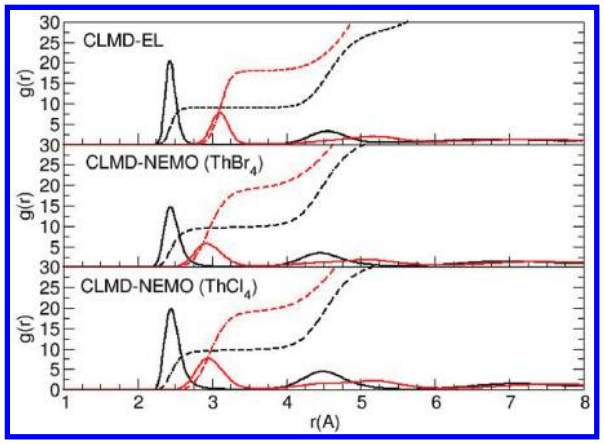

Figure 4. Th−water radial distribution function obtained from CLMD-EL and CLMD-NEMO simulations (this last for 0.1 m concentration). Th−O in black and Th−H in red. The integrated coordination numbers are also shown (dashed lines).

distribution function shown in ref 46. A similar small peak at about the same distance was observed in the case of doubly charged uranium oxocations,[19,90] and for some triply charged bare cations, like lanthanoids,[8,9,91] actinoids,[20] or Al^{3+},[92] reflecting the long-range electrostatic ion−water interaction.

From the peaks of the two shells, we characterized the hydration, and from the integrals of each shell, we obtained the coordination number (CN). In Table 2, the results are summarized and compared with previous theoretical and experimental data. The CPMD results depend on the initial conditions (i.e., initial coordination number). This is expected, since the first hydration shell water exchange time-scale is longer than the available simulation time-length (tens of picoseconds). It is thus possible to have systems trapped in a metastable state. In fact, when starting with eight and nine water molecules in the first shell, we do not see any exchange and a constant CN. On the other hand, when starting with CN = 10, the system quickly moves to CN = 9 (this is accomplished in less than 1 ps in the equilibration step). In the following, we adopt the notation CPMD-9 for simulations where the initial CN was 9 and CPMD-10 for simulations where the initial CN was 10 even if this last will give as equilibrated results a CN of 9 and differences between two simulations result very small. By comparing distances for simulations having a final CN of 8 and

Table 2. Hydration Structure around Th(IV) in Water[a]

	$r_{Th-O}^{(1)}$ (Å)	$CN^{(1)}$	$r_{Th-O}^{(2)}$ (Å)	$CN^{(2)}$
CPMD-8	2.46(8)	8	4.5(3)	16(1)
CPMD-9	2.49(9)	9	4.6(3)	18(1)
CPMD-10	2.48(9)	9	4.6(3)	18(1)
CLMD-EL	2.45(6)	9.0(1)	4.55(25)	18(1)
CLMD-NEMO ($ThBr_4$ 0.1 m)	2.45(9)	9.5(4)	4.47(25)	21(1)
CLMD-NEMO ($ThCl_4$ 0.1 m)	2.45(9)	9.6(4)	4.5(3)	21(1)
CLMD-NEMO ($ThBr_4$ 0.8 m)	2.46(10)	11.4(3)	4.5(3)	29(1)
CLMD-NEMO ($ThCl_4$ 0.8 m)	2.47(10)	11.2(3)	4.5(3)	29(1)
CLMD[c]	2.44/2.47	8.05/8.45		
CLMD[d]	2.54	9	4.75	18.9
EXAFS[e]	2.45(1)	10(1)		
EXAFS[f]	2.451(3)	9	4.657(8)	
HEXS[g]	2.46(1)	10.1(3)		

[a] $r^{(1)}$ and $r^{(2)}$ are the first and second peaks of Th−O radial distribution functions and $CN^{(1)}$ and $CN^{(2)}$ the coordination numbers of the first and second hydration shell, respectively. [b] [b]Uncertainties on simulation distances are obtained from radial distribution function fwhm. Experimental errors are reported as in the original papers. It is difficult to compare them, since Torapava et al.[45] report an error of 1σ, while others do not specify the error (probably 3σ). [c]Molecular dynamics of Réal et al.[12] [d]Molecular dynamics of Yang et al.,[48] where the first shell is rigid. [e]EXAFS experiments of Moll et al.[44] [f]EXAFS experiments of Torapava et al.[45] [g]HEXS experiments of Wilson et al.[46]

9 with the experimental values, it is not possible to make a final decision on the CN that better agrees with literature data, since the differences are largely inside the uncertainties (and fluctuations) of DFT-based simulations.[93]

Note that no hydrolysis during the CPMD simulations was observed. With the same CPMD setup, we previously studied the hydration of Po^{4+} in water,[94] for which we observed successive hydrolysis starting from a fully protonated metal aquaion (the pK_a of Po^{4+} was evaluated to be very low). In their study of the water exchange mechanism, Hartmann et al.[95] found that, for systems with a pK_a of about 2, the mechanism occurs without activation. On the other hand, in cases like La^{3+} (with a valence shell isoelectronic to that of Th^{4+}), Gd^{3+}, or Cm^{3+} in water, no spontaneous hydrolysis was reported.[18,35,36,41] For a pK_a of about 3,[45] we do not expect spontaneous hydrolysis. Moreover, in a study of a series of indicators, Simon et al.[96] showed that spontaneous deprotonation occurs in a short simulation time scale only when the pK_a is lower than the pH of the solution by more than one pH unit. Here, hydrolysis will result in a pH of 0 (one H^+ in 64 water molecules), and thus, having a pK_a of 3, we do not observe any spontaneous hydrolysis in simulations as expected. More precisely, the dissociation fraction in finite simulations can be estimated from the pK_a using formula 4 from Doltsinis and Sprik.[97] Evaluated for the CPMD setup, we find a dissociation fraction around 3%, which is then very small. The protonated complex is thus largely predominant, and we thus do not expect to observe spontaneous dissociation in the time scale simulated.

CLMD results, both with the NEMO and EL approaches, are in good agreement with experimental distances. The predicted coordination numbers are 9.5 and 9, respectively. In the NEMO simulations, the value of 9.5 corresponds to an equilibrium between 9- and 10-coordinated Th. Note that

dx.doi.org/10.1021/jp210350b | J. Phys. Chem. B 2012, 116, 6465−6475

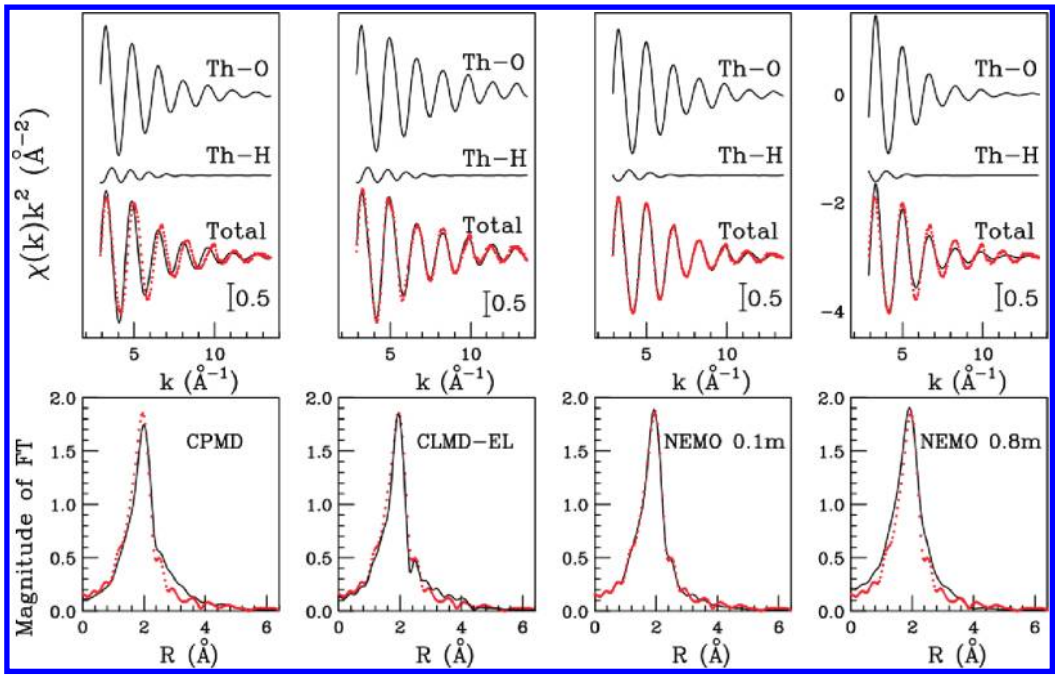

Figure 5. Upper panels: Comparison between the EXAFS theoretical signals (solid black line) calculated from the CPMD, CLMD-EL, and NEMO Th−O and Th−H $g(r)$'s and experimental data (dotted red line). Lower panels: Non-phase-shifted corrected Fourier transforms of the experimental data (dotted red line) and of the theoretical signals (solid black line).

this value was already suggested by Soderholm and co-workers from integrating the number of electrons contributing to the scattering pair from HEXS experiments.[46] From CLMD-EL simulation, we also observed some exchanges between CN = 9 and CN = 10 with a predominance of CN = 9, as shown in Figure S3 in the Supporting Information, which provides an average CN of 9.0 ± 0.1.

A direct comparison of the MD structural results with the EXAFS experimental data allows us to determine the Th(IV) hydration geometry with high accuracy. To this end, $\chi(k)$ theoretical signals were calculated by means of eq 5 for all simulations from Th−O and Th−H $g(r)$'s. The structural parameters derived from the simulations were kept fixed during the EXAFS analysis, while the value of E_0 was 4.0 ± 0.5 eV above the first inflection point of the experimental spectrum in all cases. This procedure allowed us to compare the first hydration shell structure obtained from the simulations directly to the experimental data, and assess the validity of the theoretical frameworks.

The degree of agreement between experiments and simulations was evaluated by means of eq 6. In Table S2 in the Supporting Information, we report the R values (eq 6) for all simulations. Among Car−Parrinello simulations, CPMD-10 is the one in best agreement with experiments (we remind that it provides as equilibrated results CN = 9 and also R is not so different from CPMD-9 which also gives CN = 9 and similar distance). Concerning NEMO simulations, the 0.1 m concentration provides the best agreement. Note that the higher concentration simulations are in worse agreement with experiments (Table S2, Supporting Information). In the upper part of Figure 5, the comparison between the experimental signal and the theoretical curves is reported thus for the CPMD-10 (the signal corresponding to CPMD-9 is also not different; we report only one CPMD result for clearness), CLMD-EL, and CLMD-NEMO at both concentrations. In each panel, the first two curves from the top are the Th−O and Th−H first shell theoretical contributions calculated from the MD $g(r)$'s, while the lower curve represents the total theoretical signal compared with the experimental spectrum. The corresponding Fourier transform (FT) moduli of the theoretical and experimental spectra calculated in the interval k = 2.8−13 Å^{-1} with no phase shift are shown in the lower panels of Figure 5. The agreement between the EXAFS spectrum and the calculated curves is satisfactory for all simulations, and particularly for the NEMO simulation at 0.1 m concentration (we will discuss concentration effects in the next section). The major difference between EXAFS experimental and CPMD theoretical signals consists of a longer Th−O distance, responsible for a phase difference and consequently a displacement of the first peak in the FT. However, compared with previously reported CPMD studies of cations (Co^{2+}, La^{3+}, and Cm^{3+}) in water,[18,36,98] the agreement between simulations and experiments is satisfactory. Both classical results, using the EL and NEMO potential, are in good agreement with the experimental data.

3.2. Concentration Effects. We now discuss the role of counterions on Th(IV) hydration. For this purpose, we have employed the NEMO potential. A salt concentration increase from 0.1 to 0.8 m does not have any relevant effect on the Th−O distances, as shown from the Th−water RDFs in Figure 6. The concentration, on the other hand, has an effect on the water molecule coordination number, which increases with the concentration (from 9.5 to about 11.4 for the Br^- salt and from 9.6 to 11.2 for the Cl^- salt). The hydration structure (distances and $CN^{(1)}$'s) of Th(IV) is similar in both Cl^- and Br^- salts for 0.1 m concentration. In Figure 7, we report the coordination number as a function of time at the two concentrations. Note that, while in the case of low concentration the system is in equilibrium between $CN^{(1)}$ = 9 and $CN^{(1)}$ = 10, at higher concentration, more coordination numbers become accessible between 10 and 12. Note that in this latter case noninteger $CN^{(1)}$'s are possible for each individual frame, since they are an

dx.doi.org/10.1021/jp210350b | J. Phys. Chem. B 2012, 116, 6465−6475

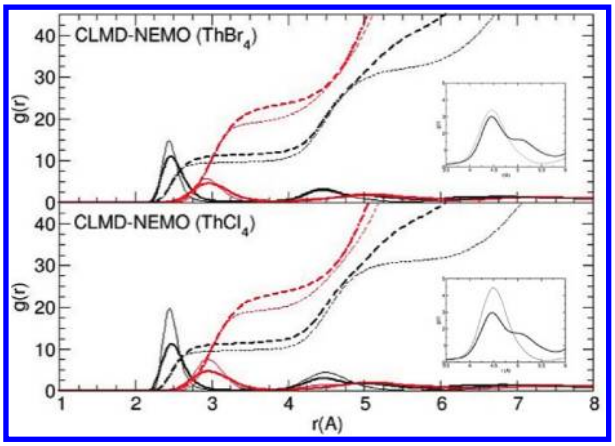

Figure 6. Th−water radial distribution function obtained from $ThBr_4$ and $ThCl_4$ simulations at high concentration (0.8 m). Th−O in black and Th−H in red. Results for the low concentrations are shown in thin lines for direct comparison. The integrated coordination numbers are also shown (dashed lines). Details on the Th−O second hydration shell $g(r)$ are reported as insets for high and low (thin lines) concentrations.

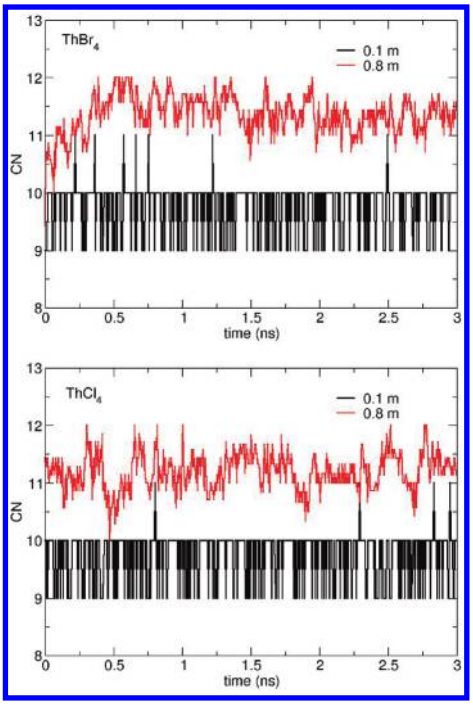

Figure 7. Water in the Th^{4+} first hydration shell (CN) as a function of time.

average over seven Th(IV) ions. A possible explanation for the increase of $CN^{(1)}$'s with concentration can be provided by inspecting the position of the anions.

Figure 5 shows a comparison between the theoretical and experimental EXAFS signals for highly concentrated simulations. The agreement (see Table S2 in the Supporting Information) is similar to the one obtained for CPMD and CLMD-EL simulations in the absence of counterions, and it is slightly worse than the one obtained for low concentration solutions. The Fourier transform of the EXAF signal shown in Figure 5 is wider when increasing the anion concentration in the simulations.

This discrepancy with experiments performed at a relatively high ClO_4^- concentration may be due to the fact that in our simulations we use a different anion than the one used experimentally, or it may be due to the force field that we employed. In any case, these differences are small and do not affect the first hydration shell distance, which is in agreement with EXAFS. Moreover, in water solutions, EXAFS is known to be able to determine the first shell distance with high accuracy. On the other hand, EXAFS is not very sensitive to coordination numbers. This is in agreement with our observations: the Th−O first shell distance does not change in the concentration range we studied, while a variation is found for the first shell coordination number.

In Figure 8, the Th−Br and Th−Cl radial distribution functions show that both Br^- and Cl^- are not in the first shell.

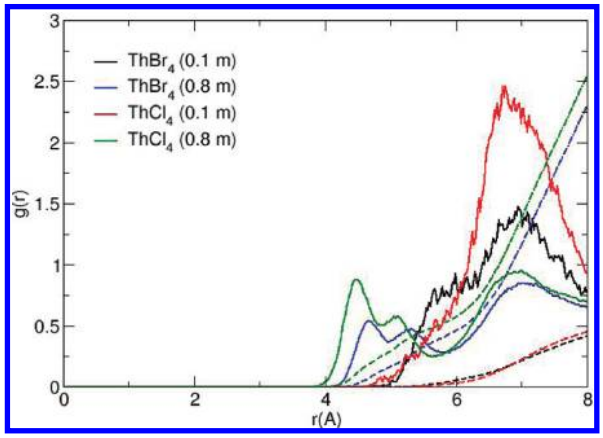

Figure 8. Th−Br and Th−Cl radial distribution functions at different concentrations. Coordination numbers are also shown in dashed lines.

Details on the minimum cation−anion distances are presented in Figure S4 of the Supporting Information. These results were obtained after equilibrated 3 ns time length simulations, starting from an initial random disposition of cations, anions, and water molecules. We also performed some simulations in which one or two anions were initially placed in contact with Th^{4+} (for both low and high concentrations and for both Cl^- and Br^-), but also in these cases, after a few ps, the anions leave the first shell. The Th−X $g(r)$ shows a peak at about 4.5 Å followed by a shoulder corresponding to the anion in roughly the second hydration shell of Th(IV). Thus, the anions are always placed in the outer sphere. At high concentration, the anions enter the second coordination sphere of Th(IV), forming "solvent separated ion pairs" (SSIP). The close proximity of the ions, especially given the high charge of Th(IV), has an effect on the water structure locally that leads to the $CN^{(1)}$ increase.

We now discuss the second-hydration-shell properties. First, we notice that $CN^{(2)}$ considerably increases at high concentration, as reported in Table 2. The relatively high $CN^{(2)}$ = 29 value is not due to a plateau in the running coordination number (see Figure 6 and details in Figure S6, Supporting Information), but it rather corresponds to the CN value at the distance where a flat region is observed in the diluted simulations. The second hydration shell is affected by the formation of solvent separated ion pairs beyond 5 Å distance from Th(IV). In fact, inspecting the integrated $g(r)$ of Figure 6 (i.e., the number of water molecules as a funciton of distance from the ion), we see that up to 5 Å both high and low dilution simulations have the same water density (about 0.05

dx.doi.org/10.1021/jp210350b | J. Phys. Chem. B 2012, 116, 6465−6475

molecules/Å^3). From 5.5 Å, they diverge, since in the case of high dilution it almost reaches a plateau and then the density decreases up to 0.037 Å^{-3} at 6 Å, while for low dilution water molecules forming the previously mentioned shoulder still increases the total number of them. The presence of many ions (more cations and anions at similar distance from cations) attracts water molecules more than isolated ions such that at 6 Å the water density at low dilution is 30% bigger than that at high dilution (and we do not observe any plateau in the $g(r)$ integral). We also inspected in more detail the Th−O distances in the second hydration shell. The shoulder in $g(r)$ at ca. 5.1 Å is due to some water molecules, which are both in the first shell of the anion (see details in Figure S7, Supporting Information) and also in the second hydration shell of Th^{4+}. Furthermore, some of the water molecules in the second hydration shell of one Th^{4+} can be at the same time in the first hydration shell of another Th^{4+}. They are in each second hydration shell 6.4% on average and thus contribute to the shoulder in the second hydration shell (see details in Figure S8, Supporting Information).

This picture explains why by increasing the total salt concentration we have that the equilibrium between free species and formation of SSIP-like species is shifted toward these lasts: a mere increase of salt concentration leads through the mass action law to an increase of dimers formed, here as solvent separated ion pairs, following the Le Chatelier principle. Thus, modifying the water activity by changing the salt concentration still results in an increase of water molecules in the cation hydration shells, since in solution the SSIP-like species should have a higher affinity to the solvent. On the other hand, when performing simulations of $ThCl_4$ at the same concentration (1.83 m) of Johansonn et al. experiments,[47,99] we found Cl^- in the first shell at a distance of 2.9−3.0 Å forming ion pairs (see Figure S5, Supporting Information), thus confirming their original conclusions but only for such a very high concentration.

Finally, by looking at the details of Th−X $g(r)$'s, we note that Cl^- anions are slightly more structured around Th(IV) than Br^- anions. At high concentration, the probability of finding Cl^- ions in the same place where the second hydration shell water molecules are (at about 4.5 Å, the Th−Cl RDF peak reaches almost 1) is about 50% more than the probability of finding Br^- at the same position (here the Th−Br RDF peak is about 0.5).

4. CONCLUSIONS

We have used different molecular dynamics techniques and *ab initio* calculations (DFT and MP2 based) coupled with EXAFS data analysis, to unravel the hydration properties of Th(IV) in liquid water. Overall, satisfactory agreement on the structural properties of Th(IV) in water was found between EXAFS experiment and theory. Among the different simulation methods, the NEMO potential, obtained from fitting ab initio interaction curves, gives the best agreement with experiment and is used for the subsequent analysis.

In liquid water, the first hydration shell Th−O distance is 2.45 Å (as previously suggested) and the coordination number is between 9 and 10, in line with recent findings on light lanthanoids(III) where for La^{3+} a 10-fold structure is dynamically accessible, while the 9-fold coordination is predominant.[5] In the case of Th^{4+}, the 10-fold structure is stabilized (probably due to the high ionic charge) and the coordination number of 9.5 results from a dynamical coexistence of the two structures for salts at high dilution.

By means of the NEMO potential, which was able to reproduce the EXAFS signal, we studied $ThBr_4$ and $ThCl_4$ concentration effects. In agreement with experimental findings, our results indicate that the anions do not perturb the Th(IV)−water distance, also at relatively high concentrations, while increasing the salt concentration has an effect on the coordination number due to the increasing probability of the anions to be in the outer sphere of the cation.

■ ASSOCIATED CONTENT

Supporting Information

Optimized structures and additional results. This material is available free of charge via the Internet at http://pubs.acs.org.

■ AUTHOR INFORMATION

Corresponding Author

*E-mail: gagliard@umn.edu.

Notes

The authors declare no competing financial interest.

■ ACKNOWLEDGMENTS

We thank Prof. I. Persson for collecting data and graciously making the raw experimental X-ray absorption spectrum available to us.

R.S. and R.V. thank ANR 2010 JCJC 080701 ACLASOLV (Actinoids and Lanthanoids Solvation) for partial support. We acknowledge GENCI (grants x2010071870 and x2011071870) for computing time. L.G. was supported by the Chemical Sciences, Geosciences, and Biosciences Division of the Office of Basic Energy Sciences of the Department of Energy under grant USDOE/DE-SC002183. C.B. thanks the HPC-EUROPA2 project (project number: 228398), with the support of the European Community - Research Infrastructure Action of the FP7.

■ REFERENCES

(1) Ohtaki, H.; Radnai, T. *Chem. Rev.* **1993**, *93*, 1157−1204.
(2) Marcus, Y. *Chem. Rev.* **1988**, *88*, 1475.
(3) Hofer, T. S.; Tran, H. T.; Schwenk, C. F.; Rode, B. M. *J. Comput. Chem.* **2003**, *25*, 211.
(4) Helm, L.; Merbach, A. E. *Chem. Rev.* **2005**, *105*, 1923−1959.
(5) Duvail, M.; Souaille, M.; Spezia, R.; Cartailler, T.; Vitorge, P. *J. Chem. Phys.* **2007**, *127*, 034503.
(6) Duvail, M.; Vitorge, P.; Spezia, R. *J. Chem. Phys.* **2009**, *130*, 104501.
(7) Duvail, M.; Spezia, R.; Vitorge, P. *ChemPhysChem* **2008**, *9*, 693−696.
(8) Floris, F. M.; Tani, A. *J. Chem. Phys.* **2001**, *115*, 4750−4765.
(9) Meier, W.; Bopp, P.; Probst, M. M.; Spohr, E.; Lin, J. L. *J. Phys. Chem.* **1990**, *94*, 4672−4682.
(10) Kowall, T.; Foglia, F.; Helm, L.; Merbach, A. E. *J. Phys. Chem.* **1995**, *99*, 13078−13087.
(11) Duvail, M.; Ruas, A.; Venault, L.; Moisy, P.; Guilbaud, P. *Inorg. Chem.* **2010**, *49*, 519.
(12) Réal, F.; Trumm, M.; Vallet, V.; Schimmelpfennig, B.; Masella, M.; Flament, J.-P. *J. Phys. Chem. B* **2010**, *114*, 15913−15924.
(13) Frick, R.; Pribil, A. B.; Hofer, T. S.; Randolf, B. R.; Bhattacharjee, A.; Rode, B. M. *Inorg. Chem.* **2009**, *48*, 3993.
(14) Beuchat, C.; Hagberg, D.; Spezia, R.; Gagliardi, L. *J. Phys. Chem. B* **2010**, *114*, 15590−15597.
(15) Villa, A.; Hess, B.; Saint-Martin, H. *J. Phys. Chem. B* **2009**, *113*, 7270.
(16) Yang, T.; Bursten, B. E. *Inorg. Chem.* **2006**, *45*, 5291.

(17) Hagberg, D.; Bednarz, E.; Edelstein, N. M.; Gagliardi, L. *J. Am. Chem. Soc.* **2007**, *129*, 14136.
(18) Atta-Fynn, R.; Bylaska, E. J.; Schenter, G. K.; de Jong, W. A. *J. Phys. Chem. A* **2011**, *115*, 4665.
(19) Hagberg, D.; Karlstrom, G.; Roos, B. O.; Gagliardi, L. *J. Am. Chem. Soc.* **2005**, *127*, 14250−14256.
(20) Duvail, M.; Martelli, F.; Vitorge, P.; Spezia, R. *J. Chem. Phys.* **2011**, *135*, 044503.
(21) Clavaguera, C.; Calvo, F.; Dognon, J.-P. *J. Chem. Phys.* **2006**, *124*, 074505.
(22) Clavaguera, C.; Pollet, R.; Soudan, J. M.; Brenner, V.; Dognon, J.-P. *J. Phys. Chem. B* **2005**, *109*, 7614.
(23) Clark, A. *J. Chem. Theory Comput.* **2008**, *4*, 708−718.
(24) Schreckenbach, G.; Shamov, G. A. *Acc. Chem. Res.* **2010**, *43*, 19−29.
(25) Siboulet, B.; Marsden, C. J.; Vitorge, P. *Chem. Phys.* **2006**, *326*, 289−296.
(26) Den Auwer, C.; Guillaumont, D.; Guilbaud, P.; Conradson, S. D.; Rehr, J. J.; Ankudinov, A.; Simoni, E. *New J. Chem.* **2004**, *28*, 929−939.
(27) Shamov, G. A.; Schreckenbach, G. *J. Phys. Chem. A* **2005**, *109*, 10961−10974.
(28) Hay, P. J.; Martin, R. L.; Schreckenbach, G. *J. Phys. Chem. A* **2000**, *104*, 6259−6270.
(29) Spencer, S.; Gagliardi, L.; Handy, N. C.; Ioannou, A. G.; Skylaris, C.-K.; Willets, A.; Simper, A. M. *J. Phys. Chem. A* **1999**, *103*, 1831−1837.
(30) Wiebke, J.; Moritz, A.; Cao, X.; Dolg, M. *Phys. Chem. Chem. Phys.* **2007**, *9*, 459−465.
(31) Toraishi, T.; Tsuneda, T.; Tanaka, S. *J. Phys. Chem. A* **2006**, *110*, 13303−13309.
(32) Siboulet, B.; Marsden, C. J.; Vitorge, P. *New J. Chem.* **2008**, *32*, 2080−2094.
(33) Kuta, J.; Clark, A. *Inorg. Chem.* **2010**, *49*, 7808−7817.
(34) Dinescu, A.; Clark, A. *J. Phys. Chem. A* **2008**, *112*, 11198−11206.
(35) Ikeda, T.; Hirata, M.; Kimura, T. *J. Chem. Phys.* **2005**, *122*, 244507.
(36) Terrier, C.; Vitorge, P.; Gaigeot, M.-P.; Spezia, R.; Vuilleumier, R. *J. Chem. Phys.* **2010**, *133*, 044509.
(37) Buhl, M.; Kebrede, H.; Diss, R.; Wipff, G. *J. Am. Chem. Soc.* **2006**, *128*, 6357−6368.
(38) Buhl, M.; Kebrede, H. *ChemPhysChem* **2006**, *7*, 2290−2293.
(39) Nichols, P.; Bylaska, E. J.; Schenter, G. K.; De Jong, W. *J. Chem. Phys.* **2008**, *128*, 124507.
(40) Spezia, R.; Siboulet, B.; Abadie, S.; Vuilleumier, R.; Vitorge, P. *J. Phys. Chem. B* **2011**, *115*, 3560−3570.
(41) Yazyev, O. V.; Helm, L. *J. Chem. Phys.* **2007**, *127*, 084506.
(42) *The Use of Thorium as Nuclear Fuel*; American Nuclear Society: 2006.
(43) MacKay, D. J. C. *Sustainable Energy - without the hot air*; UIT Cambridge Ltd.: 2009.
(44) Moll, H.; Denecke, M. A.; Jalilehvand, F.; Sandstrom, M.; Grenthe, I. *Inorg. Chem.* **1999**, *38*, 1795−1799.
(45) Torapava, N.; Persson, I.; Eriksson, L.; Lundberg, D. *Inorg. Chem.* **2009**, *48*, 11712−11723.
(46) Wilson, R. E.; Skanthakumar, S.; Burns, P. C.; Soderholm, L. *Angew. Chem., Int. Ed.* **2007**, *46*, 8043−8045.
(47) Johansson, G.; Magini, M.; Ohtaki, H. *J. Solution Chem.* **1991**, *20*, 775−792.
(48) Yang, T.; Tsushima, S.; Suzuki, A. *J. Phys. Chem. A* **2001**, *105*, 10439−10445.
(49) Yang, T.; Tsushima, S.; Suzuki, A. *Chem. Phys. Lett.* **2002**, *360*, 534−542.
(50) Habash, J.; Smith, A. J. *Acta Crystallogr., Sect. C* **1983**, *39*, 413.
(51) Rogers, R. D. *Lanthanide Actinide Res.* **1989**, *3*, 71.
(52) Wilson, R. E.; Skanthakumar, S.; Sigmon, G.; Burns, P. C.; Soderholm, L. *Inorg. Chem.* **2007**, *46*, 2368−2372.
(53) Car, R.; Parrinello, M. *Phys. Rev. Lett.* **1985**, *55*, 2471−2474.
(54) Duvail, M.; Souaille, M.; Spezia, R.; Cartailler, T.; Vitorge, P. *J. Chem. Phys.* **2007**, *127*, 034503.
(55) Engkvist, O.; Åstrand, P. O.; Karlström, G. *Chem. Rev.* **2000**, *100*, 4087−4108.
(56) Galbis, E.; Hernandez-Cobos, J.; Den Auwer, C.; Naour, C. L.; Guillaumont, D.; Simoni, E.; Pappalardo, R. R.; Sanchez Marcos, E. *Angew. Chem., Int. Ed.* **2010**, *49*, 3811.
(57) Spezia, R.; Duvail, M.; Vitorge, P.; D'Angelo, P. *J. Phys.: Conf. Ser.* **2009**, *190*, 012056.
(58) D'Angelo, P.; Zitolo, A.; Migliorati, V.; Chillemi, G.; Duvail, M.; Vitorge, P.; Abadie, S.; Spezia, R. *Inorg. Chem.* **2011**, *50*, 4572−4579.
(59) Troullier, N.; Martins, J. L. *Phys. Rev. B* **1991**, *43*, 1993−2006.
(60) Kleinman, L.; Bylander, D. M. *Phys. Rev. Lett.* **1982**, *48*, 1425−1428.
(61) Becke, A. D. *Phys. Rev. A* **1988**, *38*, 3098.
(62) Lee, C.; Yang, W.; Parr, R. G. *Phys. Rev. B* **1988**, *37*, 785.
(63) Hovey, J. K. *J. Phys. Chem. B* **1997**, *101*, 4321−4334.
(64) McQuarrie, D. A. *Statistical Mechanics*; University Science Books: Sausalito, CA, 2000.
(65) Fine, R. A.; Millero, F. J. *J. Chem. Phys.* **1973**, *59*, 5529.
(66) Nosé, S. *Mol. Phys.* **1984**, *52*, 255−268.
(67) Hutter, J.; Alavi, A.; Deutsch, T.; Bernasconi, M.; Goedecker, S.; Marx, D.; Tuckerman, M.; Parrinello, M. *CPMD*, version 3.9.1; IBM Research Division, IBM Corp and Max Planck Institute: Stuttgart, Germany, 2004.
(68) Thole, B. T. *Chem. Phys.* **1981**, *59*, 341−350.
(69) Jorgensen, W. L.; Chandrasekhar, J.; Madura, J. D.; Impey, R. W.; Klein, M. L. *J. Chem. Phys.* **1983**, *79*, 926−935.
(70) van Duijnen, P.; Swart, M. *J. Phys. Chem. A* **1998**, *102*, 2399.
(71) Souaille, M.; Loirat, H.; Borgis, D.; Gaigeot, M.-P. *Comput. Phys. Commun.* **2009**, *180*, 276−301.
(72) Sprik, M. *J. Chem. Phys.* **1991**, *95*, 2283.
(73) Essmann, U.; Perera, L.; Berkowitz, M. L.; Darden, T.; Lee, H.; Pedersen, L. G. *J. Chem. Phys.* **1995**, *103*, 8577−8593.
(74) Duvail, M.; Spezia, R.; Cartailler, T.; Vitorge, P. *Chem. Phys. Lett.* **2007**, *448*, 41−45.
(75) Duvail, M.; Vitorge, P.; Spezia, R. *Chem. Phys. Lett.* **2010**, *498*, 90−96.
(76) Karlström, G.; Lindh, R.; Malmqvist, P.-A.; Roos, B. O.; Ryde, U.; Veryazov, V.; Widmark, P.-O.; Cossi, M.; Schimmelpfennig, B.; Neogrady, P.; Seijo, L. *Comput. Mater. Sci.* **2003**, *287*, 222−239.
(77) Gagliardi, L.; Lindh, R.; Karlström, G. *J. Chem. Phys.* **2004**, *121*, 4494−4500.
(78) Linse, P.; Wallqvist, A.; Astrand, P. O.; Nymand, T. M.; Lobaskin, V.; Carlson, F. *Molsim*; Lund University: Lund, Sweden, 2003.
(79) Berendsen, H. J. C.; Postma, J. P. M.; Van Gunsteren, W. F.; Di Nola, A.; Haak, J. R. *J. Chem. Phys.* **1984**, *81*, 3684−3690.
(80) Kolafa, J.; Perram, J. *Mol. Simul.* **1992**, *9*, 351.
(81) D'Angelo, P.; Barone, V.; Chillemi, G.; Sanna, N.; Mayer-Klauke, W.; Pavel, N. *J. Am. Chem. Soc.* **2002**, *124*, 1958.
(82) Hubert, S.; Barthelet, K.; Fourest, B.; Lagarde, G.; Dacheux, N.; Baglan, N. J. *J. Nucl. Mater.* **2001**, *297*, 206−213.
(83) George, G. N.; Pickering, I. J. *EXAFSPAK - A Suite of Computer Programs for Analysis of X-Ray Absorption Spectra*; SSRL: Stanford, CA, 1993.
(84) Rehr, J. J.; Albers, R. C. *Rev. Mod. Phys.* **2000**, *72*, 621−654.
(85) Filipponi, A. *J. Phys.: Condens. Matter* **1994**, *6* (41), 8415.
(86) Filipponi, A.; Di Cicco, A.; Natoli, C. R. *Phys. Rev. B* **1995**, *52*, 15122−15134.
(87) Filipponi, A.; Di Cicco, A. *Phys. Rev. B* **1995**, *52*, 15135−15141.
(88) D'Angelo, P.; Zitolo, A.; Migliorati, V.; Persson, I. *Chem.—Eur. J.* **2010**, *16*, 684−692.
(89) Giaquinta, D. M.; Soderholm, L.; Yuchs, S. E.; Wasserman, S. R. *J. Alloys Compd.* **1997**, *249*, 142−145.
(90) Frick, R. J.; Hofer, T. S.; Pribil, A. B.; Randolf, B. R.; Rode, B. M. *J. Phys. Chem. A* **2009**, *113*, 12496−12503.
(91) Clavaguéra, C.; Calvo, F.; Dognon, J.-P. *J. Chem. Phys.* **2006**, *124*, 074505.

(92) Faro, T. M. C.; Thim, G. P.; Skaf, M. S. *J. Chem. Phys.* **2009**, *132*, 114509.
(93) Duvail, M.; D'Angelo, P.; Gaigeot, M.-P.; Vitorge, P.; Spezia, R. *Radiochim. Acta* **2009**, *97*, 339−346.
(94) Ayala, R.; Spezia, R.; Vuilleumier, R.; Martinez, J. M.; Pappalardo, R. R.; Sanchez Marcos, E. *J. Phys. Chem. B* **2010**, *114*, 12866−12874.
(95) Hartmann, M.; Clark, T.; van Eldik, R. *J. Phys. Chem. A* **1999**, *103*, 9899−9905.
(96) Simon, C; Ciccotti, G; Klein, M. *ChemPhysChem* **2007**, *8*, 2072.
(97) Doltsinis, N. L.; Sprik, M. *Phys. Chem. Chem. Phys.* **2003**, *5*, 2612−2618.
(98) Spezia, R.; Duvail, M.; Vitorge, P.; Cartailler, T.; Tortajada, J.; Chillemi, G.; D'Angelo, P.; Gaigeot, M.-P. *J. Phys. Chem. A* **2006**, *110*, 13081−13088.
(99) The simulation was performed with NEMO-FF in a box composed by 17 Th^{4+}, 68 Cl^{-}, and 497 H_2O corresponding to a concentration of 1.83 m.